Available online at www.sciencedirect.com
SCIENCE DIRECT®
ELSEVIER
Journal of Magnetism and Magnetic Materials 260 (2003) 60–69
Journal of magnetism and magnetic materials
www.elsevier.com/locate/jmmm

Magnetic properties of praseodymium ions in Na_2O–Pr_2O_3–SiO_2 glasses

A. Mekki[a,*], Kh.A. Ziq[a], D. Holland[b], C.F. McConville[b]

[a] *Department of Physics, King Fahd University of Petroleum and Minerals, Dhahran 31261, Saudi Arabia*
[b] *Department of Physics, University of Warwick, Coventry CV4 7AL, UK*

Received 17 February 2002; received in revised form 21 July 2002

Abstract

Sodium praseodymium silicate glasses of nominal composition $0.3Na_2O$ xPr_2O_3 $(0.7-x)SiO_2$, where $0 \leqslant x \leqslant 0.10$, have been studied by magnetisation and X-ray photoelectron spectroscopy (XPS). The magnetisation data fail to collapse to a single curve in the M versus H/T representation for all values of x and the spread increases with x, indicating an increase in the magnetic exchange interaction. The M versus H data acquired at different temperatures have been fitted with a Brillouin function by refining the number of Pr^{3+} ions in each glass sample. It was found that most of the Pr ions are in Pr^{3+} valence state and only a small fraction ($\leqslant 5\%$) in the Pr^{4+} state. Analysis of the XPS line shape indicates only the presence of Pr^{3+} ions in these glasses.

Keywords: Pr_2O_3; Glass; Magnetisation; X-ray photoelectron spectroscopy

1. Introduction

Oxide glasses containing small concentrations of rare earth metal oxide (<2 mol%) have been studied extensively as a consequence of their optical behaviour [1]. For example, it has been stated that there are at least 36 lasing transitions in rare earth doped glass systems [2]. The studies on larger concentrations (up to ~30 mol%) of rare earth metal oxides in oxide glasses have been reviewed by Shelby [3] and work on the magnetic behaviour in such systems has been reviewed by Moorjani and Coey [4] and Kohli [5]. Special attention has been paid to glasses containing gadolinium ions [6–8] but other rare earth ions such as europium, holmium and cerium have also been investigated. However, little work has been published on the magnetic properties of praseodymium doped oxide glasses.

In this study, we present the results from magnetisation and DC magnetic susceptibility measurements (M versus H, and χ^{-1} versus T) and X-ray photoelectron spectroscopy (XPS) of praseodymium oxide incorporated into sodium silicate glasses. The objectives of this study are first to investigate the magnetic properties of Pr ions in a random system and secondly to study the redox state of Pr ions in the sodium silicate matrix. A detailed XPS study of the sodium praseodymium silicate glasses has been published elsewhere [9].

*Corresponding author. Tel.: +966-03-860-4292; fax: +966-03-860-2293.
E-mail address: akmekki@kfupm.edu.sa (A. Mekki).

0304-8853/03/$ - see front matter
PII: S0304-8853(02)00568-1

Basic magnetic parameters (Curie temperature and effective magnetic moment) have been calculated in order to obtain qualitative information on the type and strength of the magnetic interaction. Moreover, we have performed differential thermal analysis (DTA), thermal expansion coefficient and density measurements on the amorphous network as a function of the Pr_2O_3 content.

2. Experimental details

2.1. Sample preparation

The glass samples were prepared using commercially available analytical grade powders of Pr_6O_{11} (for Pr_2O_3), Na_2CO_3 (for Na_2O) and SiO_2. Calculated amounts of these powders were mixed and melted in a 90% Pt/10% Rh crucible at 1400°C for 2 h. Each glass, obtained by fast quenching of the melt, was crushed and then remelted at the same temperature to ensure homogeneity. The final melt was then cast into preshaped graphite-coated steel moulds yielding rod specimens with dimensions $5.0 \times 5.0 \times 30\,mm^3$ for XPS analysis. No XPS and thermal expansion data were recorded from the $x = 0.10$ glass sample as it was not possible to produce glass rods for this composition. After casting, the specimens were transferred to another furnace maintained at 50°C below the glass transition temperature (T_g, as determined from the DTA trace) for 2 h before being cooled to room temperature at a rate of 30°C/h. After preparation, the samples were stored in a desiccator. The chemical composition of each sample was determined by inductively coupled plasma emission spectroscopy (ICP) and the values are listed in Table 1.

2.2. Physical properties

X-ray powder diffraction was used to check that the glasses formed were completely amorphous and the density of each glass was measured using Archimedes' principle with deionised water as the displacement liquid.

DTA measurements were made on approximately 0.1 g of sample, heated from room temperature to 1200°C at a rate of 10°C/min in a Stanton Redcroft 673-4 analyser. Crystalline alumina was used as the reference. The thermal expansion coefficients (α) were measured in a quartz push-rod dilatometer, heated from room temperature to ~600°C at 2°C/min.

2.3. Magnetic measurements

The magnetisation data, M versus T, were recorded using a 9 T variable temperature vibrating sample magnetometer (VSM) in the temperature range 2–300 K. The temperature-measuring sensor was a calibrated carbon glass resistor located near the specimen and the system was calibrated using a pure nickel standard. The overall accuracy in the temperature measurements was better than ±1% throughout the range, while that of the magnetisation measurements was estimated to be approximately ±5%.

Table 1
Nominal and analysed compositions of the praseodymium sodium silicate glasses

x	Nominal			Analysed		
	Na_2O	SiO_2	Pr_2O_3	Na_2O	SiO_2	Pr_2O_3
0.000	0.30	0.70	—	0.31	0.69	—
0.025	0.30	0.675	0.025	0.28	0.69	0.023
0.050	0.30	0.65	0.05	0.28	0.67	0.044
0.075	0.30	0.625	0.075	0.29	0.65	0.058
0.100	0.30	0.60	0.10	0.29	0.63	0.078

The relative uncertainty in the ICP results is ±5%.

2.4. XPS measurements

The XPS spectra were obtained using a VG Scientific ESCALAB Mk II spectrometer where the base pressure in the analysis chamber was maintained at $\sim 2 \times 10^{-10}$ mbar. A non-monochromatic Al K_α (1486.6 eV) X-ray source and a 150 mm concentric hemispherical analyser were used to record the C 1s, O 1s, Pr 3d, Na 1s and Si 3p core levels. For XPS measurements, a glass rod from each composition was fractured in ultra high vacuum (UHV). Each glass bar was notched to guide the fracture, held in a specially designed sample holder, and fractured in UHV to give a cleaved surface, the composition of which should be representative of the bulk composition. For consistency, all binding energies are reported with reference to the C 1 s transition at 284.6 eV, which arises from minor hydrocarbon contaminants in the vacuum system.

3. Results and discussion

3.1. Physical properties

The nominal and analysed compositions of the glasses are given in Table 1 and the densities are summarised in Table 2. The density increases with increasing Pr_2O_3 content in the glass. This is a predictable result given that Pr ions have a larger mass that Si and a higher coordination number for oxygen. All samples were X-ray amorphous within the detection limits of the technique.

The DTA trace obtained from the 10% Pr_2O_3 glass sample is shown in Fig. 1 and is typical of all the other glass compositions investigated. The glass transition, crystallisation and melting temperatures, determined from the DTA trace of each sample, are summarised in Table 2. We note an increase in the glass transition temperature with increasing Pr_2O_3 content in the glass and this is indicative of the strengthening of the glass network.

Table 2 also lists the thermal expansion coefficients (α) for the glass samples. The general trend is a decrease in TCE with increasing Pr_2O_3 content in the glass, also suggesting a strengthening of the glass structure. This would imply that Pr ions enter the glass network as intermediates, similar to the role of Al^{3+} ions in silicate-based glasses, although higher coordination numbers are expected.

No attempt was made to identify the crystalline phases formed after the heat treatment process of each glass sample. The magnetic and structural properties of the devitrified samples will be presented elsewhere.

3.2. Magnetic data

The DC magnetic susceptibility ($\chi = M/H$) values were determined by measuring the magnetisation (M) at an applied magnetic field (H) of 20 kOe as a function of temperature. The susceptibility data for the base glass doped with 0.075 Pr_2O_3 are shown in Fig. 2a as a plot of χ versus T and χ^{-1} versus T for the temperature range 4–300 K. As can be seen from this figure, the high-temperature inverse susceptibility follows a Curie–Weiss law behaviour: $\chi = C/(T - \theta_P)$ with a negative Curie temperature (θ_P). Fig. 2b shows χ^{-1} as a function of T for all glass samples investigated in the temperature range 4–300 K. The solid lines represent the Curie–Weiss law behaviour of the inverse magnetic susceptibility versus temperature, and are used to calculate the Curie constant C, Curie temperature θ_P, and the effective magnetic moment for each glass. These parameters are summarised in Table 3, where it can be seen that C increases with increasing Pr_2O_3 content in the glass and θ_P becomes increasingly more negative, going from ~ -30 to ~ -50 K as x increases from 0.023 to 0.078. The effective magnetic moment is consistent with that of Pr^{3+} ($\mu = 3.5\,\mu_B$) except for the lowest concentration $x = 0.023$ where $\mu_{eff} = 3.27\,\mu_B$.

The increasingly negative Curie temperature indicates that the magnetic exchange interaction in the glass is antiferromagnetic and increases in strength with increasing Pr_2O_3 content. The value of θ_P for the oxide Pr_2O_3 is reported to be –73 K in the low-temperature cubic phase [10]. It has been suggested that clustering of ions is required in the network if there is to be sufficient proximity to permit magnetic correlations which can account for the highly negative values of θ_P for these glass

Table 2
Thermal and physical parameters from DTA, thermal expansion and density measurements

x	$T_g \pm 1$ (°C)	$T_x \pm 1$ (°C)	$T_m \pm 1$ (°C)	α (MK^{-1}) ± 1.2	ρ (g/cm^3) ± 0.02
0.000	475	725	780	14.8	2.41
0.023	487	759.1	832	14.3	2.68
0.044	502	751.2	—	13.7	2.95
0.058	514	794.9	897	11.6	3.22
0.078	531	814	939	—	3.35

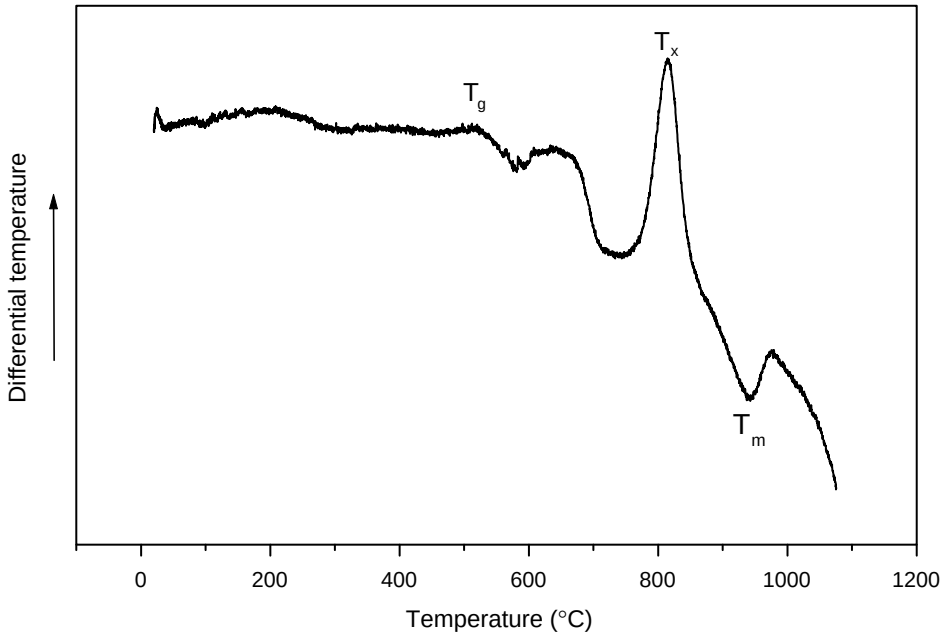

Fig. 1. DTA trace for the $0.29Na_2O_3$ $0.078Pr_2O_3$ $0.63SiO_2$ glass, showing the glass transition temperature (T_g), crystallisation peak (T_x) and the melting peak (T_m).

samples. If the ions were uniformly distributed throughout the matrix, then the mean Pr–Pr separation would range from 0.9 to 0.6 nm over the concentration range studied. This is comparable to separations of 0.5–0.35 nm in the oxide and corresponds to the Pr^{3+} ions being separated by 2 [SiO_4] tetrahedra on average. It would appear that weak spin exchange may occur over these distances, via intervening bonds, but is insufficient to produce alignment at finite temperatures.

The effect of the exchange interaction can be seen graphically by plotting M versus H/T. Magnetic measurements were performed at three or more temperatures for each sample making it possible to plot the magnetisation data as a function of H/T. Figs. 3a and b show representative data from two glasses ($x = 0.023$ and 0.044) and it can be seen that the data do not collapse onto a single curve for each glass composition but increasingly diverge as the Pr_2O_3 content increases in the glass. For paramagnetic materials, the data should collapse to a single curve, as in the case of Gd_2O_3 doped lead borate [6] and CuO doped sodium silicate glasses [11]. The divergence of these data at different temperatures supports the conclusion that the Pr ions are behaving

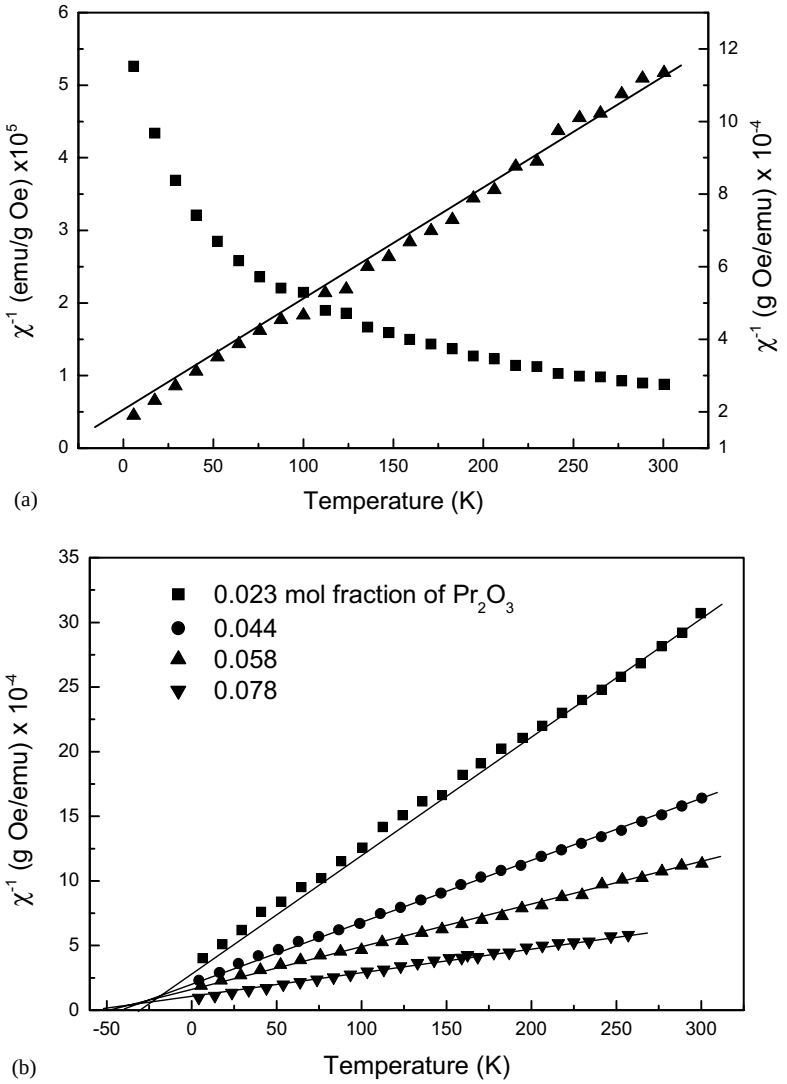

Fig. 2. (a) DC magnetic susceptibility for the $x = 0.058$ glass as plots of χ vs. T and χ^{-1} vs. T. The solid line represents the Curie–Weiss law, (b) DC magnetic susceptibility for all glass samples investigated. The solid line represents the Curie–Weiss law.

Table 3
Parameters derived from χ^{-1} versus T for the Pr_2O_3 doped glass series

x	N (10^{20}atoms/g) $\pm 5\%$	C (emu K/g Oe) $\times 10^{-3} \pm 10\%$	$-\theta_p \pm 2$ (K)	$\mu_{\text{eff}} \pm 0.15$ (μ_B)
0.023	4.2	1.0	28	3.27
0.044	7.4	2.4	32	3.56
0.058	9.2	3.5	50	3.52
0.078	11.6	5.6	52	3.50

N is the number of Pr ions per gram in each sample.

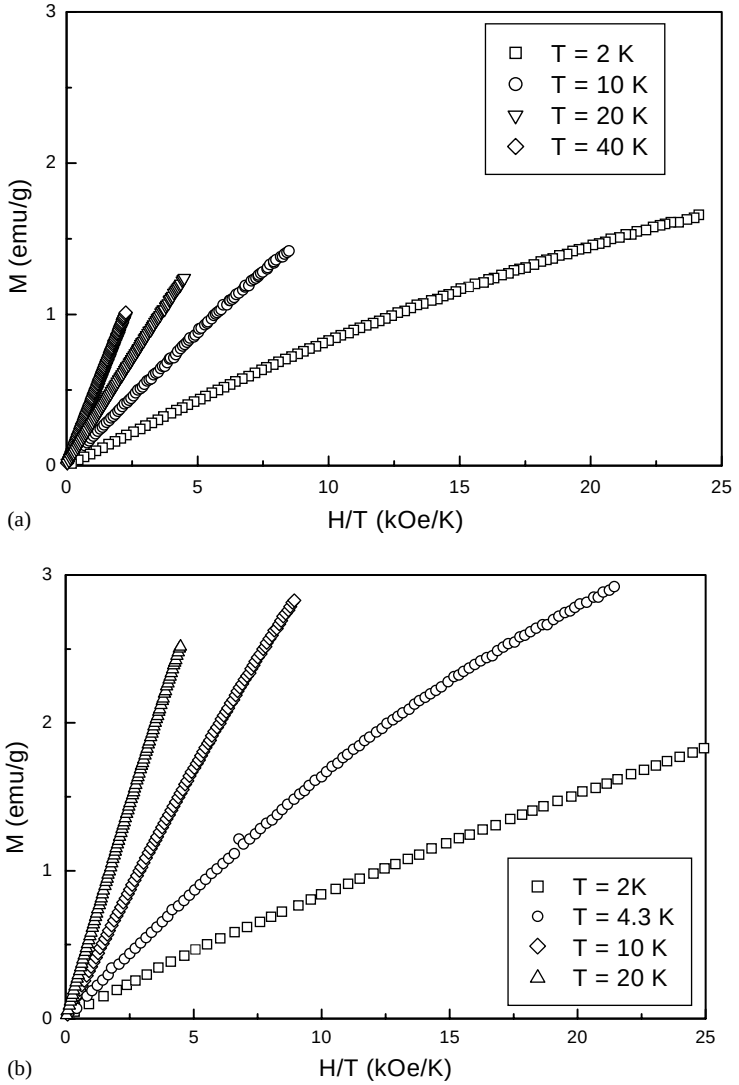

Fig. 3. Magnetisation versus H/T at different temperatures for two representative compositions: (a) $x = 0.023$ and (b) $x = 0.044$.

antiferromagnetically and that the exchange interaction increases as more Pr ions are introduced into the glass network.

The magnetic data (M versus H) was fitted by the following equation:

$$M = NgJ\mu_B B_J(x), \tag{1}$$

where

$$B_J(x) = \frac{2J+1}{2J}\coth\left[\frac{2J+1}{2J}x\right] - \frac{1}{2J}\coth\left[\frac{x}{2J}\right]$$

is the Brillouin function. M is the total magnetisation, N is the number of magnetic ions, J is the total angular momentum, μ_B is Bohr magneton and g is the Lande splitting factor.

The value of x is generally taken to be equal to $gJ\mu_B H/kT$ for a paramagnetic exchange interaction. However, in this case, the value of x is modified to $x = gJ\mu_B H/k(T-\theta)$ to take into account the exchange interaction between the Pr ions in the glass matrix, where θ takes the values

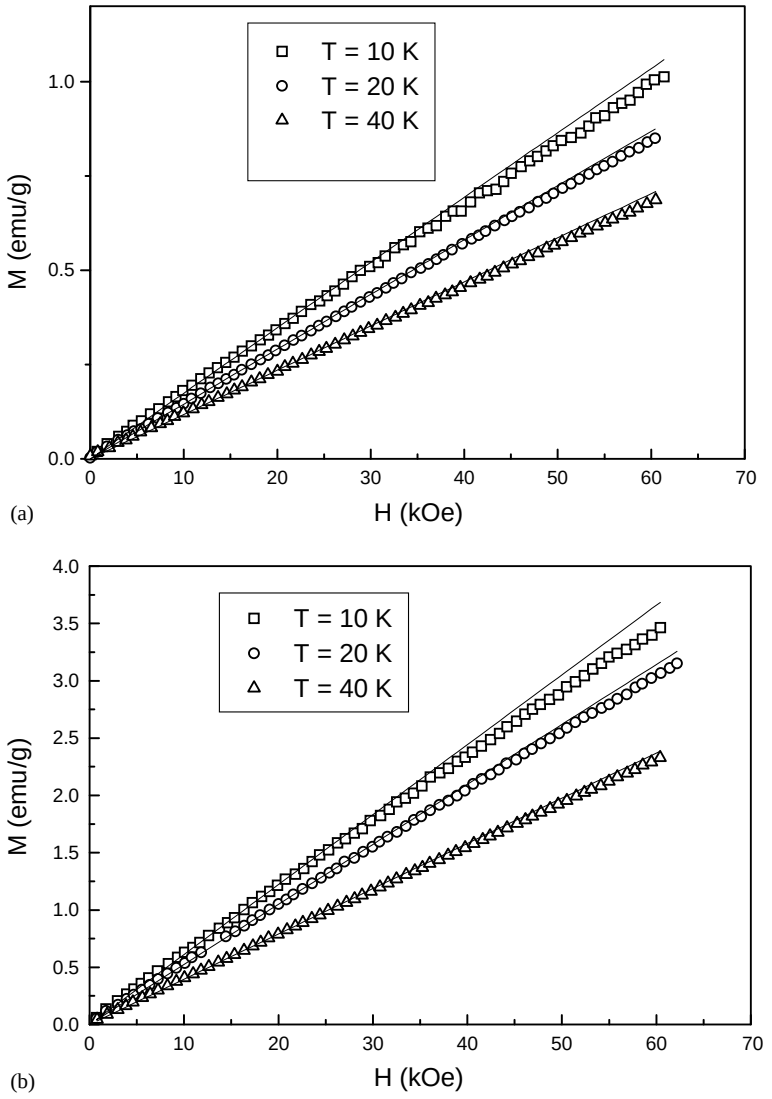

Fig. 4. Magnetisation versus magnetic field for (a) $x = 0.023$ glass and (b) $x = 0.078$ glass samples at different temperatures. The experimental data are shown by points, while the solid lines represent the fits to the data.

reported in Table 3 depending on the glass composition.

It is well known that Pr^{3+} and Pr^{4+} ions can exist simultaneously in a glass network [12] and, since they are $4f^2$ and $4f^1$, respectively, they can both contribute to the total magnetisation of the glass. Eq. (1) can therefore be rewritten as

$$M = M(Pr^{3+}) + M(Pr^{4+}) = N_1 g J_1 \mu_B B_{J_1}(x_1) + [(N - N_1) g J_2 \mu_B B_{J_2}(x_2)], \quad (2)$$

where

$$x_i = \frac{g J_i \mu B H}{k_B (T - \theta_p)}, \quad i = 1, 2.$$

For Pr^{3+}, $J_1 = |L_1 - S_1| = 4.0$ and $g_1 = 0.8$, whilst for Pr^{4+} ion, $J_2 = |L_2 - S_2| = 4.5$ and $g_2 = 0.5$ [13]. The magnetisation data for each glass sample were fitted to Eq. (2) with contributions from Pr^{3+} and Pr^{4+} ions. The number of Pr^{3+} ions/g (N_1), was used as the adjustable parameter to obtain the best

Table 4
Concentration of Pr^{3+} ions/g $\times 10^{20}$ and the ratio $[Pr^{3+}]/Pr_{total}$ needed to fit the magnetic data M vs. H for three representative temperatures for the Pr_2O_3-doped sodium silicate glasses

x	10 K		20 K		40 K	
	$[Pr^{3+}]\pm5\%$	$[Pr^{3+}]/Pr_{total}$	$[Pr^{3+}]\pm5\%$	$[Pr^{3+}]/Pr_{total}$	$[Pr^{3+}]\pm5\%$	$[Pr^{3+}]/Pr_{total}$
0.023	4.1	0.98	4.0	0.96	4.0	0.96
0.044	7.1	0.96	7.3	0.99	7.0	0.95
0.058	9.1	0.98	8.8	0.95	8.9	0.97
0.078	11.5	0.99	10.7	0.95	10.7	0.95

fit to the experimental data. Such fits are shown in Figs. 4a and b for $x = 0.025$ and 0.10 glass compositions and values of N_1 at different temperatures are shown in Table 4 and expressed also as $[Pr^{3+}]/Pr_{total} = N_1/N$. It is clear from the table that most of the Pr ions in the glasses are in the Pr^{3+} valence state. Only a small fraction (less than 5% in all samples) of Pr^{4+} exists in each glass sample and this value is of the order of the combined errors in composition and magnetisation measurement.

3.3. XPS data

In order to identify the different oxidation states of Pr ions in these glasses, it is necessary to fit the Pr 3d spectra with contributions from the two possible oxidation states of Pr, namely Pr^{3+} and Pr^{4+}. The XPS spectra of polycrystalline powders of Pr_2O_3 and PrO_2 have been previously recorded and the binding energies of the Pr $3d_{5/2}$ core level peaks were found to be 933.4 and 935.5 eV, respectively [14] with the energy separation of the Pr $3d_{3/2}$ and Pr $3d_{5/2}$ core levels being 20.7 and 17.8 eV, respectively [15]. In addition, the Pr $3d_{5/2}$ core level spectra of these two oxides exhibit a shoulder ~4–4.5 eV on the *lower* binding energy (BE) side of the metal peak. In the XPS spectra of some transition metal oxides (TMO) similar structures, called shake-up satellites, appear on the *higher* BE side of the metal peak [16]. In the case of Pr and some other rare earth metals such as Nd, the satellite structure appears on the *lower* BE side of the metal peak and is called a shake-off satellite [17]. The satellite to main peak intensity ratio for Pr_2O_3 has been observed to be 0.40 [18].

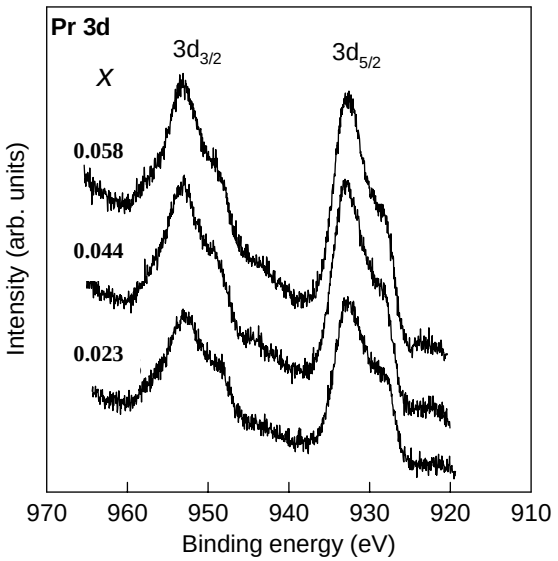

Fig. 5. A series of high-resolution XPS spectra of Pr 3d core level showing the spin–orbit splitting of the 3d level.

Table 5
Binding energy of the core level Pr $3d_{5/2}$ and its associated satellite

x	$BE_{Pr\ 3d5/2}$ (eV)	$BE_{Satellite}$ (eV)	ΔE (eV)	R (%)
0.023	933.2	929.1	4.1	35.1
0.044	933.2	929.2	4.0	35.2
0.058	933.2	929.1	4.1	34.9

ΔE is the energy separation between the main peak and the satellite. R is the ratio of the integrated intensities of the main and satellite peaks. The accuracy in the binding energies is ±0.2 eV.

The Pr 3d XPS core level spectra of the Pr_2O_3-doped glasses are shown in Fig. 5. The data for the $x = 0.10$ glass are not available as no glass rod

could be produced for this composition. The spin–orbit splitting of the 3d level is clearly seen in this figure and the Pr $3d_{5/2}$ BE is found to be constant (933.2 ± 0.2 eV) with x and the energy separation between the Pr $3d_{3/2}$ and the Pr $3d_{5/2}$ transitions is found to be 20.5 eV for all glasses. A strong shoulder can be seen on the lower BE sides of the Pr $3d_{5/2}$ and Pr $3d_{3/2}$ peaks, constant in intensity relative to the main peak. The BE of the $3d_{5/2}$ shoulder (929.1 ± 0.2 eV) and the energy separation between the main peak and the shoulder (4.0 ± 0.2 eV) are also invariant with Pr_2O_3 content in the glass. Parameters determined from these spectra are reported in Table 5 and are consistent with the presence of Pr^{3+} with no evidence of the presence of Pr^{4+} ions. An energy separation between Pr^{3+} and Pr^{4+} ions in excess of two electron volts would have been separated into two distinct contributions (the energy resolution of the instrument analyser is 1.1 eV). However, the small quantity of Pr^{4+} suggested by the magnetisation data would be difficult to detect without very much better signal-to-noise than that achievable on conventional XPS spectrometers on a reasonable time scale. Fitting of the Pr $3d_{5/2}$ to contributions from Pr^{3+} and its satellite only

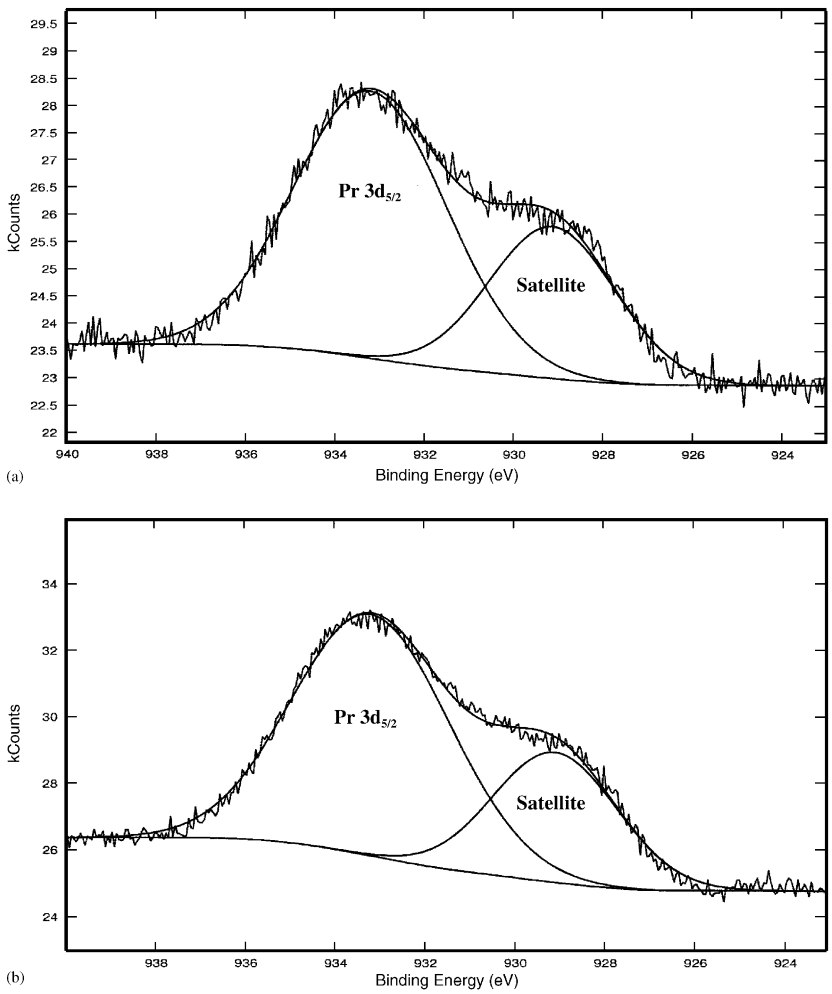

Fig. 6. The XPS Pr $3d_{5/2}$ peak for (a) $x = 0.023$ and (b) $x = 0.058$ glasses, fitted to two contributions from the main core level peak and the associated satellite.

(Figs. 6a and b) reveals no unaccounted intensity and is consistent with the results found in the literature for Pr^{3+}.

4. Conclusions

We have investigated the redox state of Pr ions in a series of praseodymium sodium silicate glasses using magnetic and XPS techniques. Magnetisation reveals that less than 5% of the praseodymium ions are present as Pr^{4+} and fracture surfaces give photoelectron spectra which can be interpreted in terms of Pr^{3+} only. The magnetic study of these glasses also reveals that the magnetic exchange interaction is antiferromagnetic and increases with increasing Pr_2O_3 content in the glass. The thermal and physical properties indicate a strengthening of the glass structure as Pr ions are introduced.

Acknowledgements

Two of the authors (A.M. and K.A.Z.) would like to acknowledge the support of King Fahd University of Petroleum and Minerals.

References

[1] A.G. Clare, in: J.E. Shelby (Ed.), Key Engineering Materials, Vol. 94–95, 1994, Trans Tech Publications, Switzerland.
[2] M.J. Weber, 93rd Annual Meeting of the American Ceramic Society, Cincinnati, Ohio, 1991.
[3] J.E. Shelby, in: J.E. Shelby (Ed.), Key Engineering Materials, Vol. 94–95, 1994, Trans Tech Publications, Switzerland.
[4] K. Moorjani, J.M.D. Coey, Magnetic Glasses, Elsevier, Amsterdam, 1984.
[5] J.T. Kohli, in: J.E. Shelby (Ed.), Key Engineering Materials, Vol. 94–95, 1994, Trans Tech Publications, Switzerland.
[6] M.A. Valente, S.K. Mendiratta, Phys. Chem. Glasses 33 (1992) 149.
[7] I. Ardelean, E. Burzo, D. Mitulesco, S. Simion, J. Non-Cryst. Solids 146 (1992) 256.
[8] E. Culea, I. Milea, J. Non-Cryst. Solids 189 (1995) 246.
[9] A. Mekki, K.A. Ziq, D. Holland, C.F. McConville, Phys. Chem. Glasses 43 (2002) 41.
[10] K.N.R. Taylor, M.I. Darby, Physic of Rare Earth Solids, Chapman & Hall, London, 1972, p. 226.
[11] A. Mekki, D. Holland, Kh.A. Ziq, C.F. McConville, Phys. Chem. Glasses 39 (1998) 45.
[12] K. Tanaka, N. Tatehata, K. Fujita, K. Hirao, J. Phys. D 31 (1998) 2622.
[13] C. Kittel, Introduction to Solid State Physics, 6th Edition, Wiley, New York, 1986.
[14] Y. Uwamino, I. Ishizuka, H. Yamatera, J. Electron. Spectrosc. Relat. Phenom. 34 (1984) 67.
[15] D.D. Sarma, C.N. Rao, J. Electron. Spectrosc. Relat. Phenom. 20 (1980) 25.
[16] D. Briggs, M.P. Seah, Practical Surface Analysis Wiley, New York, 1990, p. 130.
[17] P. Burroughs, A. Hamnet, A.F. Orchard, G. Thornton, J. Chem. Soc. Dalton Trans. 17 (1976) 1686.
[18] H. Bertout, C.K. Jorgensen, C. Bonnelle, Chem. Phys. Lett. 38 (1976) 199.